Journal of the Korean Physical Society, Vol. 42, February 2003, pp. S88∼S93

Fluorescent Ultraviolet Spectra of Molecular Hydrogen in Star Forming Clouds

Soojong Pak* and Youngsam Yu
Astronomy Program in School of Earth and Environmental Sciences, Seoul National University, Seoul 151-742†

Dae-Hee Lee and Kyung-Wook Min
Satellite Technology Research Center, Korea Advanced Institute for Science and Technology, Daejon 305-701

Ewine F. van Dishoeck
Sterrewacht Leiden, Postbus 9513, 2300 RA LEIDEN, The Netherlands

The far-UV photons from the newly born stars make Photo-dissociation Regions (PDRs) on the surfaces of the nearby molecular clouds. In the PDRs, molecular hydrogens which absorb the far-UV photons in the Lyman-Werner bands are electrically excited, and then de-excited to the ground electrical states, emitting far-UV lines. These observations are only possible from space telescopes and can be one of the scientific purposes of the first Korean scientific satellite. In order to prove the feasibility of observations for various celestial sources, we run a radiative transfer code to simulate the H_2 fluorescent lines with various physical conditions, *i.e.*, gas density, gas temperature, external far-UV field strength, and spectral energy distribution of the external UV field. The code considers bound-continuum transitions as well as bound-bound transitions. The total fluorescent intensities and the spectral shapes depend on the physical conditions. By observing the far-UV spectra from the PDRs, we can study the interaction of the young stars with the ambient clouds and the evolution process of the star forming clouds.

PACS numbers: 95.85.Mt, 97.10.Bt
Keywords: Fluorescent, Spectra, Ultraviolet, Star formation

I. INTRODUCTION

Galaxies are filled with the interstellar medium (ISM) which is the birthplace of stars. In the Milky Way Galaxy, the mass of the gas and dust is about 8×10^9 solar masses ($M_\odot$), while the total stellar mass is about 10^{11} $M_\odot$ (see the reviews in Ref. 1). The newborn stars also control the chemical and physical structures of the nearby ISM and possibly regulate the star formation efficiency [2,3].

Much of the ISM is in cold neutral medium or in gravitationally bound molecular clouds where stars form. The molecular hydrogen (H_2) is, of course, the most abundant molecules in the molecular clouds. Since hydrogen is the lightest atom, the moment of inertia of H_2 is very small, and the lowest energy levels of H_2 have excitation temperatures that are too high (*e.g.*, $\Delta E/k \simeq 500$ K for $J = 2 \rightarrow 0$) to be thermally excited in the cold ($T < 50$ K) molecular clouds. H_2 also is a homonuclear molecule whose dipole transitions in the vibration-rotation states are prohibited, and only the quadrupole transitions are allowed. The observations of the molecular clouds have been concentrated to several tracing molecules, *e.g.*, CO, CS, and HCN, even those abundances are much less than 10^{-4} of H_2. Recently, Far-Ultraviolet Spectroscopic Explorer [4] has observed H_2 absorption bands from quiescent translucent interstellar clouds whose visual extinction (A_v) is less than 2 magnitude [5–7].

The H_2 molecules on the surfaces of the Photodissociation Regions (PDRs) [1,8,9] absorb far-ultraviolet (far-UV) photons in Lyman and Werner bands and emit fluorescent emission lines in the far-UV bands [10] and in near- and mid-infrared bands [11]. The fluorescent emission in the infrared bands has been observed many times from various star forming regions in external galaxies, *e.g.*, ultraluminous in frared galaxies [12,13] and the Magellanic Clouds [14], and in the Milky Way Galaxy, *e.g.*, the Galactic center [15,16] and Orion nebula [17].

The observations of far-UV emissions from star forming clouds, however, are only accessible from space telescopes. So far only one celestial target has been observed

*Currently Visiting Assistant Professor at the Institute of Space and Astronautical Science in Japan. ; E-mail: soojong@astro.snu.ac.kr.
†The Institute of Space and Astronautical Science, Kanagawa 229-8510, Japan

from the reflection/emission nebula IC 63 [18, 19], because the emission regions from the PDRs are usually too extended to be suitable for high spatial resolution instruments. In 2003, the first Korean scientific satellite, KAISTSAT-4, will be launched with its on-board instrument, Far-ultraviolet IMaging Spectrograph (FIMS) [20–22]. FIMS will make an all-sky survey in $90-115$ nm and $134-175$ nm bands with spectral resolution of 0.15 nm. The principal mission program of FIMS is to measure hot ($T = 10^{4.5-6}$ K) plasma in the Galaxy [20,23]. The observing spectral bands and the sensitivity can also detect the H_2 Lyman-Werner band emission lines from the PDRs [24].

In this paper, we will review the PDR model and present the simulated spectra of fluorescent emission of H_2 in star forming clouds, in order to prove the feasibility of the observations for various celestial sources and to suggest possible sciences from the observations.

II. PHOTODISSOCIATION REGIONS

1. Basic Theory

The massive young stars emit intense ultraviolet (UV) radiation toward nearby molecular clouds. The UV photons whose energy is higher than the Lyman limit ($E_{photon} > 13.6$ eV) are absorbed in the H II regions, and the far-UV photons (6 eV $< E_{photon} <$ 13.6 eV) penetrate through the surfaces of nearby molecular clouds. The absorbing regions, where the far-UV photons dominate the ionization of atoms (*e.g.*, C), the formation and destruction of molecules (*e.g.*, H_2, CO), and the heating of the gas, are called *photodissociation regions* (PDRs, see the reviews in Ref. 1). In general, PDRs include most of the atomic gas in a galaxy, both in diffuse clouds and in the denser regions. In this paper, we are focusing the dense ($n_H > 10^2$ cm^{-3}) regions because in low density regions the H_2 self-shielding is not effective, and the H_2 emission may not be detectable (see the end of this Section).

In the PDRs, the external far-UV field is attenuated by dust, C, and H_2 absorptions [25]. H_2 molecules which absorb far-UV photons in the Lyman ($B^1\Sigma_u^+ - X^1\Sigma_g^+$) and Werner ($C^1\Pi^u - X^1\Sigma_g^+$) bands are electronically excited (see Figure 1). Subsequent fluorescence leads to dissociation of the H_2 molecules in about 10 % of the cases. In the remaining 90 % of the cases, the H_2 molecules de-excite, on the time scale of 10^{-8} sec, to vibrationally excited states of the ground electronic state by emitting far-UV emission lines in Lyman and Werner bands [10]. The molecules in the $X^1\Sigma_g^+$ state have various vibration-rotation energy levels, and then cascade down to the lower vibration-rotation levels on the time scale of 10^6 sec by emitting the quadrupole transitions in near- and mid-IR bands [11].

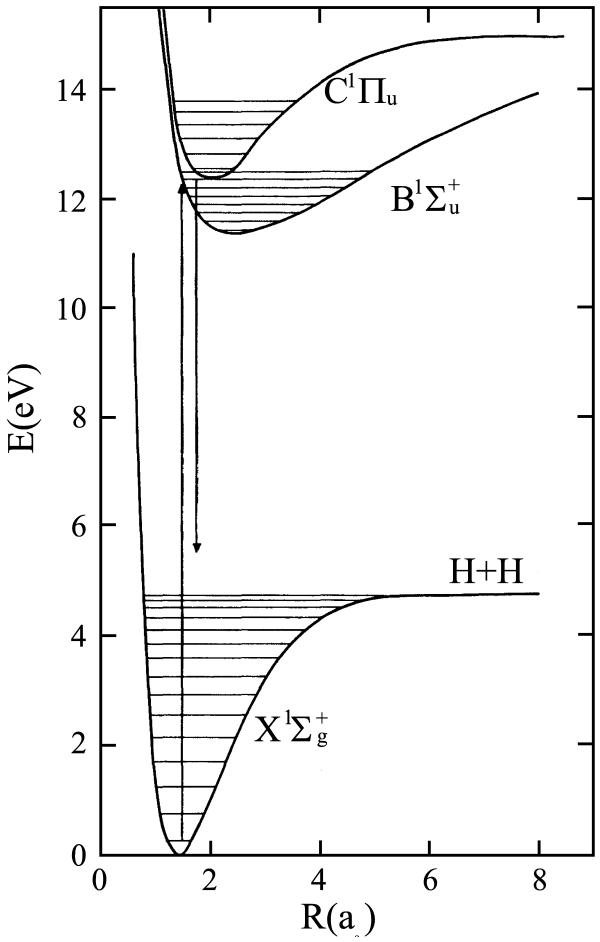

Fig. 1. Energy levels of molecular hydrogen. The transitions between the electronically excited energy levels ($B^1\Sigma_u^+$ and $C^1\Pi^u$) and the electronic ground level ($X^1\Sigma_g^+$) consist of the Lyman-Werner bands in far-UV bands. The transitions within the vibration-rotation energy levels make the quadrupole transition emission lines in near- and mid-IR bands. Also note that the transition probability follows Franck-Condon principle. This figure is adapted from Fig. 3.1 in Ref. 26.

Inside the PDRs, the external far-UV field is attenuated by dust absorption, by ionization of C, and by dissociation of CO and H_2. H_2-to-H transition layer is shallower than the C^+-C-CO layer because of H_2 self-shielding against the far-UV photons (see Figure 3 in Ref. 1). The conditions under which H_2 self-shielding is dominant over shielding by dust depend on the gas density and the external far-UV radiation fields [14,27]. The H_2 self-shielding is dominant when

$$\frac{n_H}{I_{UV}} \geq 1.3 \times 10^2, \qquad (1)$$

where n_H is the hydrogen density in units of cm^{-3}. I_{UV} is in the units of the Draine's average interstellar far-UV radiation fields [28] integrated over 91.2 nm $< \lambda <$ 113 nm, *i.e.*, $I_{UV} = 1$ means that the far-UV radiation

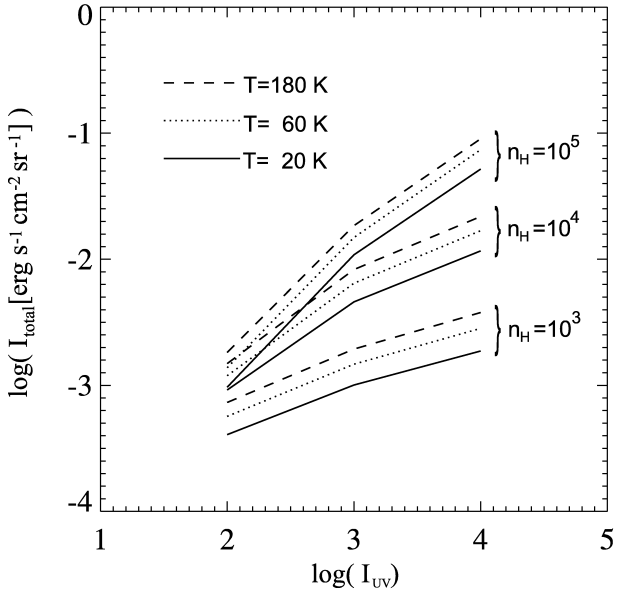

Fig. 2. Total H_2 UV fluorescent intensities for various gas temperature, gas density, and external far-UV radiation field strength.

field strength is 3.71×10^{-5} ergs s^{-1} cm^{-2} sr^{-1} [11].

2. Modeling H_2 Fluorescent Spectra

In order to simulate the H_2 fluorescent spectra in far-UV bands, we run the radiative transfer code, CLOUD [11,29–31]. The initial input parameters of the code include the hydrogen density, the cloud temperature, the grain characteristics, the H_2 formation model, and the energy spectrum and intensity of the incident UV radiation field [32].

This program considers the abundance and excitation of H_2 plane-parallel clouds. It is assumed that the abundance of H_2 is in steady state governed by the rate of formation on grain surfaces and the rates of destruction by spontaneous fluorescent dissociation following absorption in the Lyman and Werner band systems. The calculated transitions between the lowest ground state, $X^1\Sigma_g^+$, and the excited states, $B^1\Sigma_u^+$ and $C^1\Pi^u$ include *bound-continuum transitions* as well as *bound-bound transitions*. The probabilities to the continuum state are not discrete values, so standard numerical techniques, *e.g.*, a spline fit and a Simpson integration, were used in the calculations [31].

The output results from the code are dissociation and excitation rates, densities, and column densities of all vibration-rotation energy levels of H_2. The final spectrum is calculated by the Gaussian convolution program, GAUSS.

The far-UV spectral line strength is affected by foreground extinction by dust and self-absorption by H_2. We found that the extinction reduces the total H_2 fluorescent intensity by $\sim$ 15 %. But the extinction does not change the shape of the spectral profile. The total H_2 fluorescent intensity values in Table 1 (and also Figure 2) include the extinction effect, and the spectral profiles in Figures 3 and 4 do not include the extinction effect.

Table 1. Total H_2 Fluorescent Intensity in far-UV.

I_{UV} (Draine)	n_H cm^{-3}	T_{gas} K	I_{total} erg s^{-1} cm^{-2} sr^{-1}
10^2	10^3	20	4.06×10^{-4}
		60	5.67×10^{-4}
		180	7.32×10^{-4}
	10^4	20	9.18×10^{-4}
		60	1.19×10^{-3}
		180	1.49×10^{-3}
	10^5	20	9.66×10^{-4}
		60	1.38×10^{-3}
		180	1.82×10^{-3}
10^3	10^3	20	1.01×10^{-3}
		60	1.43×10^{-3}
		180	1.94×10^{-3}
	10^4	20	4.60×10^{-3}
		60	6.46×10^{-3}
		180	8.29×10^{-3}
	10^5	20	1.09×10^{-2}
		60	1.49×10^{-2}
		180	1.85×10^{-2}
10^4	10^3	20	1.87×10^{-3}
		60	2.83×10^{-3}
		180	3.78×10^{-3}
	10^4	20	1.17×10^{-2}
		60	1.69×10^{-2}
		180	2.18×10^{-2}
	10^5	20	5.18×10^{-2}
		60	7.39×10^{-2}
		180	9.03×10^{-2}

III. RESULTS AND DISCUSSIONS

1. H_2 Fluorescent Intensity

The total H_2 fluorescent line intensity in far-UV bands depends on the physical conditions of the PDR. We calculate the total intensities by changing the gas density of the PDR, n_H, the incident far-UV field radiation, I_{UV}, and the gas temperature of the PDR, T_{gas}. Table 1 and Figure 2 show the calculation results.

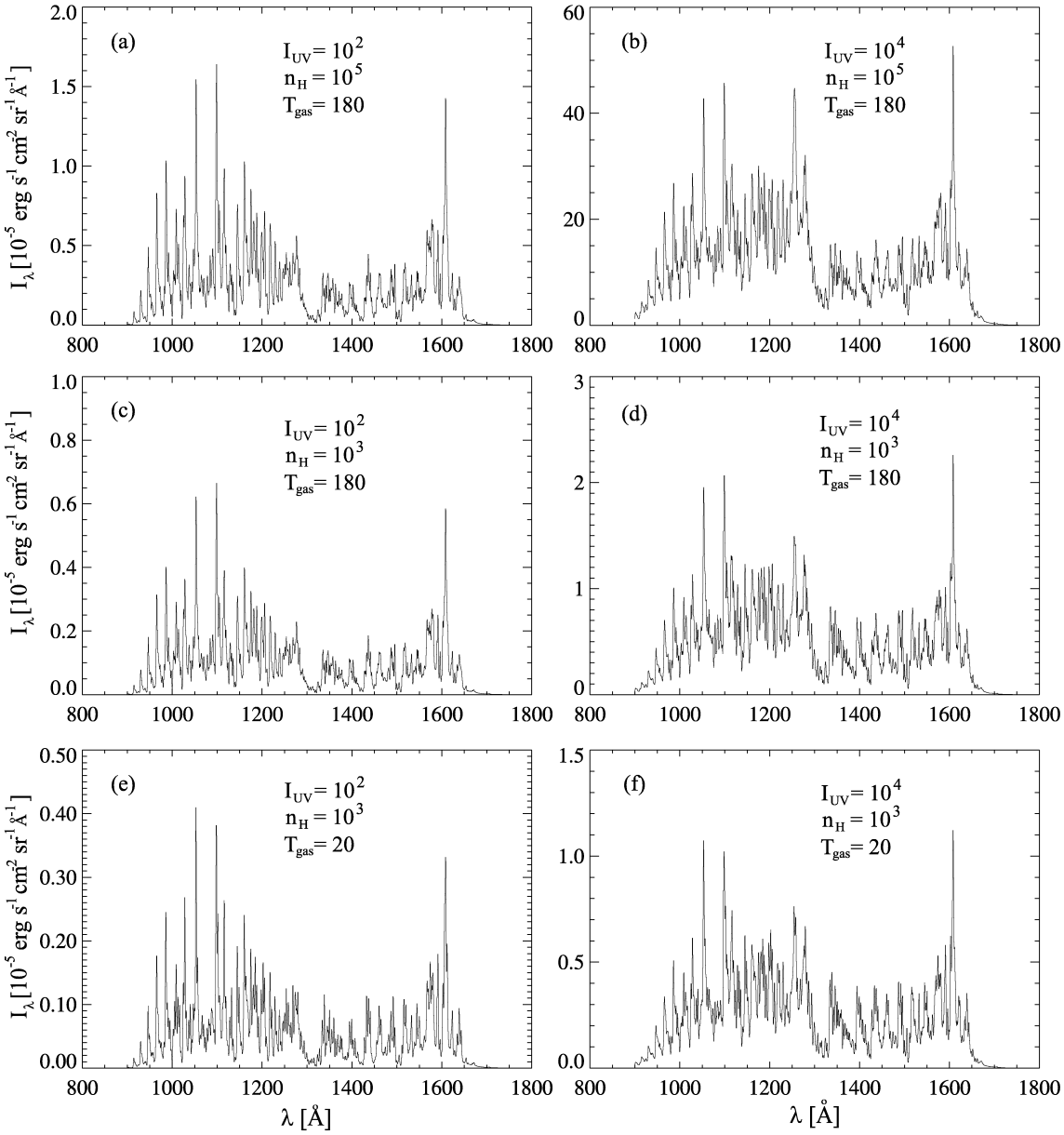

Fig. 3. Synthesized spectral shapes for various physical conditions. The line width of the Gaussian convolution process is 1.5 Å (or 0.15 nm) [21]. The units of I_{UV} is 3.71×10^{-5}ergs s^{-1}cm^{-2}sr^{-1} [11]. The spectral energy distribution of the external UV field follows the Draine's average interstellar field. The values for n_H and T_{gas} are in units of cm^{-3} and K respectively.

In Figure 2, we can see that the total fluorescent intensity of H_2 depends on the gas temperature, the gas density, and the external far-UV radiation field. Especially, when the gas density is high and the external far-UV field is low, the H_2 self-shielding dominates over the dust shielding (see Equation 1) and the H_2 fluorescent intensity is more sensitive to the external far-UV field.

The gas temperature affects the H_2 fluorescent intensity in two ways. As the gas temperature increases, the H_2 formation efficiency increases. On the other hand, the higher gas temperature causes the rotation level populations (at the $v = 0$ in $X^1\Sigma_g^+$ state) to be more distributed above the $J = 0$ level. The H_2 self-shielding becomes more important than in the lower gas temperature case.

2. Relative Line Strengths

A. Synthesized Spectrum

The H_2 fluorescent emission lines come from many bound-bound and bound-continuum transitions. The observed spectrum with a limited spectral resolution would show synthesized lines. In this work, we convolved with a spectral resolution of 1.5 Å which corresponds to the

resolution of FIMS [21]. Figure 3 shows the Gaussian convolved spectra for various input parameters.

Depending on the transient probability and the transient crowding, some spectral peaks can be seen in the spectrum. For example, the emission peaks at 1053 Å and 1099 Å represent the Werner $(0-1)$ line and the Werner $(0-2)$ line respectively. These lines are bright because the spontaneous transitions follow Franck-Condon principle [33]. On the other hand, the peak at 1608 Å is the ensemble of the Lyman $(4-11)$ line, the Lyman $(5-12)$ line, and the Lyman $(6-13)$ line [31].

B. Gas Density, Gas Temperature, and External UV

Each spectrum in Figure 3 shows the characteristics of the relative strengths of synthesized spectral lines for various physical parameters, i.e., I_{UV}, n_H, and T_{gas}. The gas density differences, as we can compare Figures 3(a) and 3(c) (or Figures 3(b) and 3(d)), do not change the features of the spectral profiles. The gas temperature also does not affect the relative line strengths, as we can see from Figures 3(c) and 3(e) (or Figures 3(d) and 3(f)).

Comparing the left plots (Figures 3(a), (c), and (e)) for $I_{UV} = 10^2$ and the right plots (Figures 3(b), (d), and (f)) for $I_{UV} = 10^4$, we can notice changes in the spectral features. At the higher external UV intensities, the 1255 Å peak by the Lyman $(1-3)$ line, the Lyman $(4-4)$ line, and the Werner $(5-9)$ line, and the 1279 Å peak by the Lyman $(0-3)$ and the Lyman $(5-5)$ line become prominent. Also the continuum features in the $1100-1300$ Å band are higher in higher I_{UV}.

C. Spectral Energy Distribution of External UV

We also calculate the H_2 fluorescent spectra for different spectral energy distributions of the external far-UV field, assuming that the external UV source is a single blackbody. Figure 4 shows the results of the blackbody radiation of $T = 10^4$ K (Figure 4(a)) and $T = 3 \times 10^4$ K (Figure 4(b)) which are similar to those of an A0 type star and a B0 type star respectively. The Draine's average interstellar far-UV radiation field, which is used in Section III-2-2, has a similar spectral shape to a B0.5 star [30].

The prominent differences between the two plots in Figure 4 are that the 966 Å peak of the Lyman $(12-0)$ line, the Lyman $(11-0)$, and the Werner $(2-0)$ line is brighter in the $T_{BB} = 3 \times 10^4$ K field, and the 1608 Å peak is brighter in the $T_{BB} = 10^4$ K field. In general, the spectral features in the shorter band $(900-1300$ Å) are brighter in the harder UV field (or in the hotter blackbody radiation), while those in the longer band $(1300-1700$ Å) are fainter.

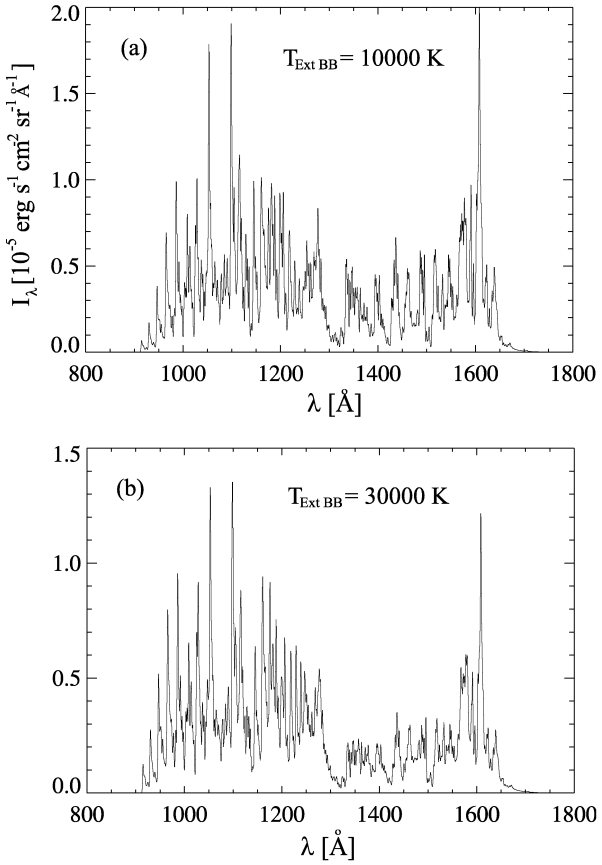

Fig. 4. Synthesized spectral shapes for different spectral energy distributions of the external UV field. The gas density, n_H, is 10^3 cm^3 and the gas temperature, T_{gas}, is 100 K. Other parameters are same as in Figure 3.

IV. CONCLUSIONS

In this paper, we present the calculation results of the H_2 fluorescent spectra in the far-UV band for different physical conditions, i.e., the gas density, the gas temperature, the external far-UV radiation field strength, and the spectral energy distribution of the external radiation field. The integrated absolute intensity and the relative strengths of the synthesized spectral lines depend on the physical conditions.

The calculation results show that FIMS survey data can detect far-UV H_2 emission from active star forming regions in our Galaxy. In order to study the regions with various star forming activity in our Galaxy and external galaxies, we may need more pointing observations. The required observing time of FIME can be estimated by using the calculation results. We can also select appropriate celestial targets for the mission programs of FIMS. We expect that the observations of FIMS can reveal the density and temperature of the gas, the population of the embedded new born stars, and the evolution stage of the star forming regions.

ACKNOWLEDGMENTS

We thank Prof. Yong-Sun Park of Seoul National University and Dr. G. van Zadelhoff of the Leiden Observatory for many helpful advices. This work was supported by the BK21 Project of the Korean Government.

REFERENCES

[1] D. J. Hollenbach and A. G. G. M. Tielens, Rev. Mod. Phys. **71**, 173 (1999).
[2] C. F. McKee, Astrophys. J. **345**, 782 (1989).
[3] F. Bertoldi and C. F. McKee, *Amazing Light: A Volume Dedicated to C. H. Townes on his 80th Birthday* (Springer, New York 1996).
[4] H. W. Moos, *et al.*, Astrophys. J. **538**, L1 (2000).
[5] J. M. Shull, *et al.*, Astrophys. J. **538**, L73 (2000).
[6] T. P. Snow, *et al.*, Astrophys. J. **538**, L65 (2000).
[7] Soon-Wook Kim, J. Korean Phys. Soc. **40**, L203 (2002).
[8] A. G. G. M. Tielens and D. J. Hollenbach, Astrophys. J. **291**, 722 (1985).
[9] K. Mockizuki and T. Nakagawa, Astrophys. J. **535**, 118 (2000).
[10] A. Sternberg, Astrophys. J. **347**, 863 (1989).
[11] J. H. Black and E. F. van Dishoeck, Astrophys. J. **322**, 412 (1987).
[12] J. Koornneef and F. P. Israel, New Astronomy **1**, 271 (1996).
[13] J. D. Goldader, R. D. Joseph, R. Doyon and D. B. Sanders, Astrophys. J. Suppl. **108**, 449 (1997).
[14] S. Pak, D. T. Jaffe, E. F. van Dishoeck, L. E. B. Johansson and R. S. Booth, Astrophys. J. **498**, 735 (1998).
[15] S. Pak, D. T. Jaffe and L. D. Keller, Astrophys. J. **457**, L43(1996).
[16] S. Pak, D. T. Jaffe and L. D. Keller, *the 4th ESO/CTIO Workshop, The Galactic Center*, edited by Roland Gredel (Astronomical Society of the Pacific, Tempe, Arizona, 1996), Vol. 102, p. 28.
[17] M. L. Luhman, D. T. Jaffe, L. D. Keller and S. Pak, Astrophys. J. **436**, L185 (1994).
[18] A. N. Witt, T. P. Stecher, T. A. Boroson and R. C. Bohlin, Astrophys. J. **336**, L21 (1989).
[19] M. Hurwitz, Astrophys. J. **500**, L67 (1998).
[20] K. -W. Min, J. Edelstein, E. J. Korpela, W. V. Dixon, J. -H. Seon, W. Han and U. -W. Nam, American Astronomical Society Meeting, **195**, 88.10 (1999).
[21] K. S. Ryu, K. -I. Seon, I. -S. Yuk, J. -H. Seon, U. -W. Nam, D. Lee, K. -W. Min, W. Han, J. Edelstein and E. J. Korpela, J. Astron. Space Sci. **17**, 67 (2000).
[22] K. -I. Seon, I. -S. Yuk, K. S. Ryu, J. -H. Park, K. Kang, H. Jin, U. -W. Nam, W. Han, K. -W. Min and J. Edelstein and E. J. Korpela, J. of Astron. Space Sci. **18**, 81 (2001).
[23] K. -I. Seon, K. S. Ryu, I. -S. Yuk, J. -H. Seon, U. -W. Nam, D. Lee, K. -W. Min, W. Han, J. Edelstein and E. J. Korpela, J. of Astron. Space Sci. **17**, 77 (2000).
[24] S. Pak, K. S. Ryu, E. J. Korpela, J. Edelstein, Y. -S. Park, Y. H. Kim, D. -H. Lee, K. -W. Min, K. -I. Seon, J. -H. Park and W. Han, J. Korean Astron. Soc. *in preparation* (2001).
[25] M. -G. Baik, J. Korean Phys. Soc. **30**, 1 (1997).
[26] E. F. van Dishoeck, *Molecular astrophysics* (Cambridge University Press, New York 1990), p. 55.
[27] M. G. Burton, D. J. Hollenbach and A. G. G. M. Tielens, Astrophys. J. **365**, 620 (1990).
[28] B. T. Draine, Astrophys. J. Suppl. **468**, 269 (1978).
[29] E. F. van Dishoeck and J. H. Black, Astrophys. J. **334**, 771 (1988).
[30] D. J. Jansen, E. F. van Dishoeck, J. H. Black, M. Spaans and C. Sosin, Astron. Astrophys. **302**, 223 (1995).
[31] C. Sosin, E. F. van Dishoeck and J. H. Black, *unpublished reports* (1990).
[32] Yunyoung Choi, Jongmann Yang and Insu Yi, J. Korean Phys. Soc. **34**, L199 (1999).
[33] J. -S. Ryu and B. S. Hudson, J. Korean Phys. Soc. **31**, 293 (1997).